

1           **The Diffuse Plate boundary of Nubia and Iberia in the Western Mediterranean: crustal**  
2           **deformation evidence for viscous coupling and fragmented lithosphere**

3  
4                           Mimmo Palano <sup>a</sup>, Pablo J. González <sup>b</sup>, José Fernández <sup>c</sup>

5  
6                           <sup>a</sup> Istituto Nazionale di Geofisica e Vulcanologia, Osservatorio Etneo - Sezione di Catania, Catania, Italy

7                           <sup>b</sup> COMET. Institute of Geophysics and Tectonics, School of Earth and Environment, University of Leeds, Leeds, United Kingdom

8                           <sup>c</sup> Institute of Geosciences, CSIC, UCM, School of Mathematics, Ciudad Universitaria, Madrid, Spain

9  
10           **Abstract**

11           A spatially dense GNSS-based crustal velocity field for the Iberian Peninsula and Northern  
12 Africa allow us to provide new insights into two main tectonic processes currently occurring in this  
13 area. In particular, we provide, for the first time, clear evidence for a large-scale clockwise rotation  
14 of the Iberian Peninsula with respect to stable Eurasia (Euler pole component: N42.612°, W1.833°,  
15 clockwise rotation rate of 0.07 deg/Myr). We favour the interpretation that this pattern reflects the  
16 quasi-continuous straining of the ductile lithosphere in some sectors of South and Western Iberia in  
17 response to viscous coupling of the NW Nubia and Iberian plate boundary in the Gulf of Cádiz. We  
18 furnish evidence for a fragmentation of the western Mediterranean basin into independent crustal  
19 tectonic blocks, which are delimited by inherited lithospheric shear structures. Among these blocks,  
20 an (oceanic-like western) Algerian one is currently transferring a significant fraction of the Nubia-  
21 Eurasia convergence rate into the Eastern Betics (SE Iberia) and likely causing the eastward motion  
22 of the Balears Promontory. These processes can be mainly explained by spatially variable  
23 lithospheric plate forces imposed along the Nubia-Eurasia convergence boundary.

24  
25           *Keywords: GNSS velocity field, crustal rotation, quasi-continuous straining, Iberia*

26  
27           **1. Introduction**

28  
29           Two end-member approaches are usually adopted to model the deformation occurring at the  
30 lithospheric scale: the block or microplate approach and the continuum model (Thatcher, 2009).  
31 The former, which is analogous to global plate tectonics, has been widely applied to model the  
32 kinematics of deformation observed at the Earth's surface (e.g., Avouac and Tapponnier, 1993).  
33 This approach emphasizes the role of the faults and discontinuous deformation in the brittle/elastic  
34 upper crust: if relative movement of rigid blocks is able to describe regional deformation, a marked

35 velocity gradient near major faults, where interseismic deficit accumulates, should be expected. The  
36 latter approach merges kinematics and dynamics under the assumption that the quasi-continuous  
37 straining of the ductile lithosphere controls the deformation (England and Jackson, 1989). This  
38 model usually assumes that the lithosphere is a uniform thin viscous sheet with no lateral or depth-  
39 wise variations in rheological properties. Although, rheological lateral variations can be added, the  
40 thin-sheet model assumes no depth variation of horizontal velocity and depth averaged values of  
41 stress. Resulting surface deformation is characterized by velocity gradients that usually are  
42 relatively smoothed in the absence of lateral viscosity variations. Although block and continuum  
43 models predict distinctly different deformation patterns and mechanical behavior, differences  
44 between their kinematics are ultimately gradual: as block size decreases and the number of faults  
45 increases, the block model approaches the deformation of a continuum, and the kinematic  
46 distinction between the two models becomes blurred.

47 The Iberian Peninsula (Fig. 1) forms the northern domain of the present-day plate boundary  
48 between Nubia (the African plate west of the East African Rift) and Eurasia in Western  
49 Mediterranean area. The GNSS (Global Navigation Satellite System) velocity field observed across  
50 this boundary (northern Morocco - southern Iberia) has been interpreted in terms of elastic block  
51 modelling (e.g., Koulali et al., 2011 and references therein). However, the detection of a significant  
52 aseismic strain component (~75%; see Stich et al., 2007 for details) suggests that relevant  
53 continuum mechanics processes cannot be ruled out. To evaluate properly those processes, which  
54 could play a significant role in the distributed regional deformation, an improved spatial resolution  
55 of the GNSS ground deformation pattern is required.

56 To this aim, here we present an analysis based on up to 15 years of GNSS observations at more  
57 than 340 sites to produce a densely spaced velocity field for whole Iberian Peninsula and Northern  
58 Morocco. We provide evidence of ongoing processes such as i) a large-scale clockwise rotation of  
59 the Iberian Peninsula with respect to stable Eurasia which can be interpreted as due to the quasi-  
60 continuous straining of the ductile lithosphere, and ii) a fragmentation of the western Mediterranean  
61 basin into several crustal blocks according to their distinct geological history.

62

## 63 **2. Background setting**

64

### 65 *2.1 Kinematics setting*

66 The movement and deformation of the Iberian Peninsula, one of the puzzling micro-plates  
67 located along the Eurasia-Africa plate boundary, has been extensively investigated by several  
68 geological and geophysical approaches. Although no consensual geodynamic model has yet been

69 achieved, these approaches coupled with studies related to large scale relative plate motions have  
70 shown that the current tectonic plate setting of the Iberian Peninsula has changed significantly over  
71 geological time (*e.g.*, [Roest and Srivastava, 1991](#); [Rosenbaum et al., 2002](#); [Platt et al., 2013](#)). In late  
72 Paleozoic times, after the Hercynian orogeny, the Iberian Peninsula was part of Pangea. Soon after  
73 the Atlantic Ocean rifting episode (~180 Ma ago), the northward propagation of the rifting process  
74 produced the eastward movement of Africa relative to Iberia-Europe and the opening of the  
75 transtensional Atlas and Betic-Rif basins (connecting the Atlantic to the Ligurian-Tethys oceanic  
76 domains) in early and middle Jurassic times respectively ([Vergés and Fernández, 2012](#) and  
77 reference therein). In early Cretaceous times, the northward propagation of the Atlantic Ocean  
78 spreading along the western margin of Iberia produced the abandonment of the Ligurian-Tethys  
79 corridor and the opening of the Bay of Biscay along the already rifted Pyrenean basin with a  
80 concurrent counter-clockwise rotation of the Iberian Peninsula (*e.g.*, [Gong et al., 2009](#); [Vissers and  
81 Meijer, 2012](#)). The progressive propagation toward north of the North Atlantic led to the  
82 abandonment of the Bay of Biscay-Pyrenean opening near the early-Late Cretaceous boundary. The  
83 Iberian Peninsula behaved as an independent micro-plate until Late Cretaceous, when Africa started  
84 to move north and northwestward relative to Eurasia (the so called Alpine Orogeny; [Moores et al.,  
85 1998](#)) The northward motion of Africa squeezed the Iberian Peninsula, producing the Pyrenees  
86 orogenic chain along its northern margin and the Betic-Rif orogen along its southern boundary.  
87 Most of the Pyrenean shortening was completed by middle Oligocene times and from this time  
88 onward the convergence of Africa was mostly accommodated across the Atlas systems (North  
89 Africa), the Betic-Rif orogenic system and within the Iberian Peninsula. The interior of the Iberian  
90 plate was deformed, inverting all previously rifted regions and producing intraplate mountain  
91 ranges (*e.g.*, [Casas-Sainz and de Vicente, 2009](#); [Gibbons and Moreno, 2002](#)). The present-day plate  
92 tectonic arrangement was reached only in the earliest Miocene, when the Iberian northern plate  
93 boundary became extinct and the peninsula became a stable part of the Eurasian plate. A  
94 tranpressive fault zone, connecting the Açores trans-tensional triple junction through the Gibraltar  
95 Orogenic Arc to the Rif and Tell-Atlas then became the main plate boundary between Africa and  
96 Eurasia in the Western Mediterranean region (*e.g.*, [McKenzie, 1970](#); [Andrieux et al., 1971](#);  
97 [Meghraoui and Pondrelli, 2012](#)).

98

## 99 2.2. Seismotectonic setting

100 The occurrence of several large earthquakes (with estimated magnitude  $M \geq 6$ ) in the last  
101 millennium on the studied area is well documented in the historical records ([Fig. 2a](#); [Stucchi et al.,  
102 2013](#); [www.emidius.eu/SHEEC/sheec\\_1000\\_1899.html](http://www.emidius.eu/SHEEC/sheec_1000_1899.html)). The Lisboa area has been hit by large

103 earthquakes ( $M \geq 6.4$ ) in 1344, 1531, 1858 and 1903, while the November 1, 1755 ( $M_w=8.7$ ) and the  
104 February 28, 1969 ( $M_w=8.0$ ) earthquakes, both striking the Gulf of Cádiz (Fig. 2a), were the largest  
105 historical events occurred in the region. Other large earthquakes ( $M \geq 6.4$ ; Stucchi et al., 2013) are  
106 located along the Betics in southern Iberia (e.g., 1522, 1680, 1748, 1829, 1884, and 1954) along  
107 northern Morocco (1079, 1623, 1624, 1909 and 2004) and along northern Algeria (1365, 1716,  
108 1819, 1825, 1858, 1867, 1891, 1910, 1922, 1954, 1980 and 2003). Large earthquakes ( $M \geq 6.0$ )  
109 occurred also along the Pyrenees in 1373, 1428 and 1660 (Stucchi et al., 2013).

110 Since 2000, more than 5300 earthquakes with magnitude  $M \geq 2.5$  were located in the NW  
111 Africa-Iberia area. Considering the distribution of instrumental seismicity (Fig. 2a), it is well  
112 documented that all the borders of the Iberian Peninsula are characterized by a diffuse seismicity,  
113 while on the central sector of the peninsula seismicity wanes. The bulk of instrumental seismicity is  
114 concentrated along the WSW-ENE regional-scale structures in northern Algeria and the easternmost  
115 Atlantic Ocean (Gulf of Cádiz), well marking two segments of the Nubia-Eurasia plate boundary. In  
116 northern Algeria, earthquakes have hypocentral depths shallower than 20 km and are characterized  
117 by fault plane solutions with prevailing reverse and subordinately strike-slip faulting style (Fig.  
118 2a,b). In the Gulf of Cádiz, earthquakes have intermediate hypocentral depths and are characterized  
119 by fault plane solutions having reverse and strike-slip features (Fig. 2a,b). Across the Gibraltar  
120 Orogenic Arc, the majority of shallower earthquakes are concentrated in the Betics and Rif  
121 mountain belts. Seismicity at intermediate-depth is concentrated along a mainly N-S trend spanning  
122 the Alboran Sea and dipping southward from crustal depths beneath the Betics to a depth of ~150  
123 km beneath the basin centre. Occasional very deep and large magnitude earthquakes (~650 km)  
124 occur under the Central Betics (Buforn et al., 2004).

125

### 126 3. GNSS data processing and velocity field computation

127 Here we analyze an extensive GNSS dataset covering approximately 15 years of observations,  
128 from 1999.00 up to 2014.68, at all continuous sites where data are openly shared. The dataset  
129 includes 280 continuous GNSS sites available at the EUREF Permanent Network  
130 ([www.epncb.oma.be](http://www.epncb.oma.be)), at the Crustal Dynamics Data Information System (<http://cddis.nasa.gov>) and  
131 from various networks developed on the Iberian Peninsula by local institutions and agencies mainly  
132 for mapping, engineering and cadastral purposes. In addition to continuous GNSS sites, we  
133 included data from 25 episodic GNSS sites located in Morocco (see Koulali et al., 2011 for details)  
134 with surveys spanning the 1999.80-2006.71 time interval, whose raw observations are available  
135 through the UNAVCO archive ([www.unavco.org](http://www.unavco.org)). We have updated and extended previous studies  
136 (e.g., Fernandes et al., 2007; Koulali et al., 2011; Palano et al., 2013; Echeverría et al., 2013; Gárate

137 [et al., 2014](#)) with more than 110 new stations having times series longer than 2.5 years, especially  
138 from Portugal, northern Iberia and western Pyrenees. The GNSS data were processed by using the  
139 GAMIT/GLOBK software ([www-gpsg.mit.edu](http://www-gpsg.mit.edu)), by adopting the strategy described in Appendix A  
140 of the Supplementary material section (see also [Palano, 2015](#) for additional details). By using the  
141 GLORG module of GLOBK, all the GAMIT solutions and their full covariance matrices are  
142 combined to estimate a consistent set of positions and velocities in the ITRF2008 reference frame  
143 ([Altamimi et al., 2012](#)).

144 To improve the detail of the geodetic velocity field over the studied area, we perform a rigorous  
145 integration of our solutions with those reported in [Serpelloni et al. \(2007\)](#), [Koulali et al. \(2011\)](#),  
146 [Echeverría et al. \(2013\)](#) and [Gárate et al. \(2014\)](#). In particular, since our solutions and the published  
147 ones share several common stations, we aligned their velocities to our ITRF2008 solution by  
148 applying a Helmert transformation, obtained by solving for the transformation parameters that  
149 minimize the RMS of differences between velocities at common sites. The average discrepancies  
150 are small, and the RMS velocity difference for the common stations is less than 0.4 mm/yr. The  
151 resulting velocities and their  $1\sigma$  uncertainties, aligned to the ITRF2008 are reported in [Table S1](#).

152 To adequately show the crustal deformation pattern over the investigated area, we align our  
153 ITRF2008 GPS velocities to a fixed Eurasian reference frame ([Cannavò and Palano, 2015](#); see also  
154 [Table S1](#) and [S2](#) of the supplementary material section). The resulting velocity field, with error  
155 ellipses at the 95 per cent confidence level, is shown in [Fig. 3](#).

156 It is well regarded that the formal, standard error of the GNSS solution underestimates the true  
157 uncertainty in the GNSS velocities. Roughly speaking, the error spectrum for most stations is  
158 usually represented by a combination of seasonal signal, white noise and flicker noise (see  
159 [supplementary material for details](#)). To properly infer valuable information about the crustal motion  
160 currently occurring on the studied area, the noise effects on velocity estimates need to be taken into  
161 account. To this aim, we account for temporally correlated noise in each continuous GNSS time  
162 series by using the first-order Gauss-Markov extrapolation (FOGMEX) algorithm proposed by  
163 [Herring \(2003\)](#) to determine a random-walk noise term, which we then incorporated into the  
164 Kalman filter used to estimate the velocities. For the episodically measured sites, a random-walk of  
165 1.5 and 2.5 mm yr<sup>-0.5</sup>, representing the average values obtained for all continuous GNSS stations  
166 analyzed in this study, were added to the assumed error in horizontal and vertical positions,  
167 respectively. The adopted strategy is described in detail in the Supplementary material section  
168 (Appendix A).

169 Moreover, the simple visual inspection of velocity field reported in [Fig. 3](#) evidences that some  
170 stations show random velocities (differences of about 0.5-1 mm/yr) with respect to nearby sites.

171 This aspect could be mainly related to the monument instability of the station. In particular, a  
172 number of the analyzed GNSS networks has been developed to support commercial applications,  
173 such as mapping and cadastral purposes and stations are characterized by a wide variety of different  
174 monument types. Pillars, or steel masts, anchored to buildings represent the largest number, while  
175 monuments directly founded on consolidated bedrock are present in minor percentage. Hence, the  
176 observed geodetic monument instability is due to varying conditions of the anchoring media (*e.g.*,  
177 soil, bedrock, building, etc.) coupled with local processes (*i.e.*, soil humidity content, water table  
178 level changes, bedrock thermal expansion, etc.).

179

#### 180 **4. Results**

181 The dense spatial coverage of our geodetic velocities, comprising over 380 stations, allow us to  
182 detect for the first time a significant large-scale clockwise rotation of the southern (*i.e.*, central and  
183 western Betics) and the western (*i.e.*, western Portugal) sectors of the Iberian Peninsula. In  
184 particular, the stations located in central and western Betics move toward WSW with rates of  $\sim 1.1$   
185 mm/yr; the stations located in SW Iberia moves mainly toward NW with rates of  $\sim 3$  mm/yr, while  
186 stations located in central and northern Portugal move northwards with rates of  $\sim 1$  mm/yr. The  
187 spatially smooth SW-Iberia clockwise crustal deformation pattern suggests a rigid rotating  
188 lithosphere block. Therefore, to test such hypothesis, we estimated the Euler vector components  
189 (latitude and longitude of pole, rotation rate) for the Iberian block by using the PEM2 software  
190 (Cannavò and Palano, 2015). We started by solving for Iberia's angular velocity w.r.t. the fixed  
191 Eurasian reference frame considering a total of 229 GNSS sites distributed over the whole Iberian  
192 Peninsula with the exclusion of sites located on Balears and south-eastern Betics because their  
193 proximity to active faults. Then, we estimated recursively the Euler vector components for the  
194 Iberian block by excluding all the stations rejecting the null hypothesis based on the F-ratio criteria  
195 (see Appendix A of the Supplementary material section and Table S2). A final set of 189 sites infer  
196 a pole ( $N42.612^\circ$ ,  $W1.833^\circ$ ) that is located closely to the northwestern sector of the Pyrenean  
197 mountain range and is characterized by a clockwise rotation rate of  $0.07$  deg/Myr (Fig. 3). No  
198 significant residuals remain in the pole computation;  $\sim 80\%$  of the 189 sites show residuals lower  
199 than  $0.75$  mm/yr, evidencing that the estimated pole reasonable describes the observed geodetic  
200 velocity field.

201 Eastern Betics (*e.g.*, Almería-Murcia region) show a deformation pattern that strongly differs  
202 from the one observed for surrounding areas. In particular, geodetic velocities clearly show a NW-  
203 to-NE fan-shaped pattern with rates ranging from  $\sim 3$  mm/yr near the coast to  $\sim 0.8$  mm/yr inland  
204 (Fig. 3). The Balears promontory shows a motion that is comparable with the one detected by

205 easternmost stations located on Eastern Betics but differs from the one observed along the Catalan  
206 coastal range (northeastern Iberia) suggesting the possible presence of a distributed shear zone on  
207 the Valencia trough accounting for a general left-lateral motion (Fig. 3).

208 Stations located on the southern sector of Betics moves toward SW; this, coupled with the NW  
209 motion of stations located in eastern Rif clearly, depicts a NNW-SSE to N-S contraction of the  
210 Alboran Basin. Moreover, the western sector of the Alboran Basin seems subject to an E-W  
211 elongation due to the westward motion of stations located on the central sector of the Gibraltar Arc.  
212 A differential motion of ~0.3 mm/yr between the stations located externally and internally this area  
213 can be recognized, resulting into a minor E-W contraction of the arc (Fig. 3).

214

215

## 216 **5. Discussion**

217 In the following we discuss the main findings and their implications for regional and local  
218 deformation processes.

219

### 220 *5.1. Large-scale clockwise rotation of the SW and W boundaries of Iberian Peninsula*

221 As previously described, stations located in south-western and western Iberia show a  
222 characteristic and significant pattern of motion, while stations installed in the remaining part of  
223 Iberia lack any significant residual motion with respect to stable Eurasia. This last feature has been  
224 observed in previous GNSS-based studies estimating the Euler pole parameter for the Eurasian  
225 Plate (*e.g.*, [Nocquet and Calais, 2003](#); [Altamimi et al., 2012](#); [Palano et al., 2013](#)), while the large-  
226 scale clockwise rotation of southern and western Iberia has been never identified due to the limited  
227 coverage of GNSS stations on these areas in the past, and eventually due to the small magnitude of  
228 the crustal deformation.

229 In the previous section, we reported that stations located along southern and western Iberia can  
230 be represented with a clockwise rotating rigid block model. This large-scale rotation is consistent  
231 with those detected by paleomagnetic measurements in Neogene sedimentary basins located in the  
232 central and western Betics (*e.g.*, [Mattei et al., 2006](#) and references therein) while is two orders of  
233 magnitude smaller than those estimated by [Meghraoui and Pondrelli \(2012\)](#) along the NW Africa -  
234 Iberia plate boundary. However, the northern and eastern borders of an Iberian block cannot be  
235 clearly determined, nor does the current seismicity seem to indicate clear styles of deformation at its  
236 edges. Therefore the limits of such lithospheric block are not clear, and perhaps not represented as  
237 sharp fault bounding systems. An hypothesis would be to expect that the observed block comprises  
238 the whole Iberian Peninsula (as a microplate). However, a rotating rigid block model would predict

239 significant shortening and left-lateral shear along the Western (off-shore Lisbon) and pure  
240 shortening at the North Iberian margin (uplift of the Cantabrian Mountains and North Spain  
241 Hercynian Massif plateau?). In addition, an Iberian rotating block would require S to W motion of  
242 NE and Eastern sectors of the Iberian Peninsula (Catalonia, Aragon and Valencia), which currently  
243 velocities in this section behave consistently with respect to stable Eurasia within the error ellipses.  
244 This suggests that despite the good agreement of the best-fitting model provided by our estimated  
245 pole, a rigid rotating block with net (fault bounded) limits is unlikely to fully explain the  
246 deformation process in SW and Western Iberia as a whole. Alternatively and or in addition, the  
247 lithosphere is likely undergoing distributed deformation in some sectors of south and western Iberia,  
248 and/or unknown off-shore margin structures (e.g., Gulf of Cádiz) would be currently accumulating  
249 significant interseismic strain.

250 In [Fig. 4](#) we applied a median filter to all stations within 1x1 degree grid in order to better  
251 highlight this pattern (gray vectors). We filter the velocity field by computing the median value  
252 location of all stations to represent the vector position, and then vector magnitudes corresponding to  
253 the median values of East-West and North-South components of the velocity field for all stations  
254 within a grid cell. [Fig. 4](#) shows a representation of the interaction between the Nubia-Eurasia  
255 convergence and the residual motion w.r.t. Eurasia of the SW and W stations in Iberia. The different  
256 predicted vectors (blue arrows) differ significantly for the expected relative convergence motion  
257 between Nubia and Eurasia plates (red arrows). Moreover, we note that the azimuth of small circles  
258 around both poles, and hence the predicted motion, aligned along a NE-SW striking line crossing  
259 central Spain. This direction intersects the Nubia-Eurasia plate boundary around the Gulf of Cádiz  
260 (west of Gibraltar to the Gorringe Bank). However, the magnitude of the vector velocities disagrees  
261 by about 60%. This feature can be interpreted as the result of a significant viscous coupling of the  
262 Nubia-Eurasia convergence motion around the Gulf of Cádiz plate boundary region. In [Fig. 5a](#) and  
263 [5b](#), a SW-NE profile showing perpendicular motion component of stations from South-western  
264 Iberia to NE Spain shows a characteristic decay, which could be consistent with models of parallel  
265 velocity over wide shear strain-rates of continental deformation (e.g., [England et al., 1985](#);  
266 [Whitehouse et al., 2005](#)). Such models predict an approximate exponential decay away from the  
267 plate boundary ( $V_y \simeq V_o e^{-x/\lambda}$ ), with a length scale  $\lambda \sim L / (2\pi \sqrt{n})$ , where  $L$  is the finite length of plate  
268 boundary and  $n$  is an exponent that synthesizes the characteristics of a power-law rheology of the  
269 continental lithosphere.

270 As we estimated previously the only plate boundary segment with parallel vectors for the SW  
271 Iberia pole and the Nu-Eu pole is the Gulf of Cádiz region ([Fig. 4](#)). Therefore, we can assume that  
272 the Gulf of Cádiz is the most important segment imposing parallel traction to the plate boundary,



273 and we limit its dimensions from the Gibraltar Strait to the Gorringe Bank, with a maximum length  
274 of 450 km. As seen in Fig. 5a, this model is a first order approximation consistent with the observed  
275 velocity pattern. Exploring the parameters of this expression to fit the observed velocities along the  
276 selected profile, suggest that  $n$  is poorly constrained within values ranging from  $n=1$  to  $n=10$ . In  
277 general, if  $n$  increases the model predicts shorter  $L$  distances ( $L \leq 100$  km). Although,  $L$  can be  
278 numerically small to obtain decay rates consistent with the observed parallel velocities, we favor a  
279 longer segment to explain the observed velocity decay not only in the analyzed profile but also as  
280 an explanation for most SW Iberia region. An alternative is to consider a box-car boundary  
281 condition for the applied tangential plate boundary force. Such boundary conditions decrease  
282 significantly the length scale as  $\lambda = L/(4\sqrt{n})$ , (Whitehouse et al., 2005). Consequently, the power-  
283 law index needed to fit the observations increases to  $n \sim 3-5$  for reasonable  $L$  values ( $\sim 400-500$  km).  
284 We acknowledge, however, that a wide range of model parameters can be chosen to fit the  
285 observations (Fig. 5c and 5d).

286 The main difficulty to constrain the model parameter space is the possible interactions with the  
287 Alborán block and the lack of observations near the expected plate boundary at the Gulf of Cádiz,  
288 e.g., the SWIM structure (Zitellini et al., 2009), in an offshore region. Indeed, the observations  
289 along the profile coincide with the length scales for which the exponential decay resembles, within  
290 the observed errors, a linear decay. As a result, the current observations still not completely unique  
291 to reject rigid block rotations. Moreover, it is plausible that both processes coexist to explain the  
292 observed perpendicular velocity decay (Fig. 5a), with a long-wavelength linear trend from an  
293 inferred Iberian rotation block superimposed to the near plate boundary shear drag. Therefore, to  
294 solve this question future seafloor geodetic observations must be considered. In addition, more  
295 advanced two-dimensional physical modeling is currently under development to gain insights of the  
296 whole pattern of observations of this complex plate boundary. Although non-unique, simulations  
297 based on reasonable values, as shown above, suggest that observations can be partially explained  
298 using a simple physical model, without invoking undefined lithosphere block fault/deformation  
299 systems.

300

## 301 5.2. Crustal motion of the Balears promontory

302 Another interesting feature well recognized on the dense geodetic velocity field is the different  
303 motion between the Balears promontory (BaIP in Fig. 1) and the Catalan coastal range (NE Iberia,  
304 CCC in Fig. 1) that suggests the presence of a shear zone on the Valencia Trough accounting for a  
305 left-lateral motion (Fig. 6). Seismic reflection profiles and bathymetric surveys carried out across  
306 the whole Valencia Trough have highlighted the presence of some extensional faults along the

307 Catalan coastal range and the northwestern margin of the trough and contraction structures along  
308 the Balears promontory (*e.g.*, [Perea et al., 2012](#)). Geological evidence of Holocene activity on  
309 these faults suggests that they can accommodate the observed left-lateral motion between the  
310 Balears promontory and the Catalan coastal range ([Perea et al., 2012](#)). Moreover, the observed  
311 ENE motion of the Balears promontory seems to be related to the present-day Eastern Betics  
312 deformation process (see section 5.3.), therefore suggesting a structural and kinematic linkage with  
313 the left-lateral strike-slip Trans-Alboran Shear Zone, a NE-SW trending tectonic lineament that cuts  
314 across the southeastern margin of the Iberian Peninsula, through Eastern Betics, and crosses the  
315 Alboran Basin ([Fig. 6](#)). Since stations located on the Sardinian-Corsica block show no significant  
316 residual motion with respect to stable Eurasia (see [Palano, 2015](#)), this motion seems to be entirely  
317 absorbed within the Liguro-Provençal basin. Furthermore, the differential motion between the  
318 Balears promontory and the northern Algerian margin suggests that a small fraction of the general  
319 NW-SE Iberia-Nubia oblique convergence could be absorbed as right-lateral motion along the NE-  
320 SW-oriented Emile Baudot Escarpment (EBE in [Fig. 6](#)), which is considered as the surface  
321 expression of a lithospheric right-lateral strike-slip fault system related to the boundary between the  
322 continental crust of the Balears promontory and the thin oceanic crust of the Algerian basin  
323 ([Acosta et al., 2002](#); [Mauffret et al., 1992](#)). Such a right-lateral motion is clearly recognized also  
324 when the velocity field is referred to the Nubia plate (see [Fig. S2](#) in the supplementary material),  
325 since the motion of the Balears promontory show an oblique relationship ( $\sim 80^\circ$ ) with respect to the  
326 average strike ( $\sim N40^\circ E$ ) of the Emile Baudot Escarpment. Based on the simple vectorial  
327 decomposition of the velocities, referred to both Nubia and Eurasia reference frames, of stations  
328 located on western and central Balearic, we estimated a right-lateral motion ranging in between 0.8  
329 - 1.5 mm/yr. Additionally, a differential motion among the islands of the promontory, related to a  
330 right lateral motion on an en-echelon array of NW-SE faults cross-cutting the promontory (*e.g.*,  
331 [Acosta et al., 2002](#); [Sánchez-Alzola et al., 2014](#)) can be recognized ([Fig. 6](#)). All these features,  
332 coupled with the presence of inherited lateral lithospheric shear structures (*e.g.*, [Sanz de Galdeano,](#)  
333 [1990](#) and references therein) lend credit to a crustal segmentation of this sector of the  
334 Mediterranean Sea.

335

### 336 5.3. Crustal deformation of Betics

337 Eastern Betics are characterized by geodetic velocity vectors arranged into a WNW-to-NE  
338 fan-shaped pattern ([Fig. 6](#)). This pattern, which was previously described in [Echeverría et al.](#)  
339 ([2013](#)), depicts a prevailing NNW-SSE crustal contraction of the area in agreement with the main

340 thrusting regime inferred by geological and seismological observations (e.g., [Palano et al., 2013](#);  
341 [González et al., 2012](#), and reference therein; [Fig. 2](#)).

342 The contraction seems accommodated by a diffuse array of left-, right-lateral strike-slip and  
343 reverse faults, belonging to the “Trans-Alboran” and “Eastern Betics” shear Zones (e.g. Carboneras  
344 fault, Palomeras fault, Alhama de Murcia fault; see [Echeverría et al., 2013](#) for additional details).  
345 We suggest that such crustal contraction is related to an independent tectonic block which, trapped  
346 within the Nubia-Iberia collision, transfers a fraction of the convergent rate occurring along the  
347 westernmost Algerian margin (Oran-Chlef region; [Fig. 6](#)) into Eastern Betics. The lack of high  
348 quality P-wave tomography extensively covering the area does not allow us to put constraints on its  
349 size and shape, however recent geological and geophysical data collected along the southern margin  
350 of the Algerian basin clearly show the existence of an independent oceanic-type crustal block  
351 ([Medaouri et al., 2014](#)).

352 Another interesting feature recognized in our geodetic velocity field is the sharp change in  
353 velocities of central Betics with respect to easternmost Betics which depicts a westward relative  
354 motion of the former area and induces a crustal extension closely to Sierra de Filabres - Almería  
355 regions ([Fig. 6](#)). This extension pattern have prevailing E-W features and well agree with normal  
356 faulting inferred by mapped normal faults ([Sanz de Galdeano et al., 2012](#)) and focal mechanism  
357 solutions (see [Fig. 2b](#) for details), both having planes with prevailing N-S attitude. This extensional  
358 area has been recently indicated as the eastern edge of a crustal block which is affected by  
359 delamination processes by [De Lis Mancilla et al., \(2013\)](#). These authors indicated the external front  
360 of Betics as the northern boundary of this crustal block, however our data suggests that ~2 mm/yr of  
361 differential right-lateral motion appear to be accommodated within this block, along an E-W trans-  
362 tensional deformation zone connecting the Sierra Nevada region to Cádiz across the Granada Basin  
363 and the external Betics ([Martínez-Martínez et al. 2006](#)). The western sector of this E-W trans-  
364 tensional deformation zone spatially agrees with the northern boundary of a much larger Alboran  
365 block proposed by [Koulali et al. \(2011\)](#).

366

#### 367 *5.4. Crustal deformation of Alboran Basin*

368 As can be observed in [Fig. 3](#) the Alboran Basin is not directly sampled by geodetic  
369 observations, but valuable information can be inferred by considering the motion of bordering  
370 stations. In particular, considering the stations located along southern Betics and north-eastern Rif a  
371 NNW-SSE to N-S contraction at a rate of ~3.4 mm/yr of the Alboran Basin can be recognized. This  
372 contraction is coherent with long-term geological observations and geodynamic reconstructions of  
373 tectonic processes affecting this area and with the current Nubia-Eurasia convergence-rate ([Fig. 4](#)

374 and pole of rotations in [Table S1](#)). In particular, several studies have pointed out that a prevailing  
375 NNW-SSE contraction involving the entire basin and producing reverse and strike-slip faulting and  
376 related folding, started since about 8 Myr ([Bourgeois et al., 1992](#); [Campos et al., 1992](#); [Comas et al.,  
377 1999](#); [Morel and Meghraoui, 1996](#)). The tectonic activity of the Alboran Basin is proved by  
378 instrumental and historical earthquakes ([Fig. 2](#); [Palano et al., 2013](#) and references therein). Indeed,  
379 the occurrence of moderate to high magnitude earthquakes characterized by a mixture of fault plane  
380 solutions (from reverse to strike-slip to normal faulting) suggests that the general NNW-SSE to N-S  
381 contraction is currently partitioned by some primary crustal/lithospheric tectonic structures (*e.g.*,  
382 Trans-Alboran Shear Zone, Yusuf Fault, [Fig. 6](#)). In addition, the differential motion between  
383 stations located along the internal zones of the Gibraltar Arc (*e.g.*, northern and central Rif) w.r.t.  
384 those located along the northern (*e.g.*, southern Betics) and southern (*e.g.*, Al-Hoceima - Melilla  
385 region) boundaries of the Alboran Basin indicate  $\sim 2.4$  mm/yr of E-W crustal stretching of the  
386 western side of the basin. The intra-basin extension is coupled with a  $\sim 0.3$  mm/yr differential  
387 motion observed between the stations located externally and internally the central sector of the Arc,  
388 which defines a gentle E-W contraction of this sector of the Arc. Overall, this pattern indicates a  
389 clockwise rotation of the western sector of the Alboran Basin and surrounding parts of the Betics  
390 and Rif domains, which began more clearly when the velocity field is referred to the Nubia plate  
391 (see [Fig. S2](#) in the supplementary material) as already evidenced in [Koulali et al. \(2011\)](#). Along the  
392 NW Nubian margin, the westward motion of the Gibraltar Arc decreases toward the south near the  
393 boundary of the Atlas system while it is abruptly confined westward by the Nekor fault, an active  
394 NE-SW left-lateral strike slip fault representing the southwestern end segment of the Trans-Alboran  
395 Shear Zone ([Fig. 3](#)). Eastward of the Nekor fault the geodetic velocity field is characterized by  
396 vectors  $\sim$ NW-oriented, indicating a convergence rate ranging from 2.5 mm/yr to 5 mm/yr across the  
397 plate boundary between Iberia and Morocco-Algeria regions in agreement with previous  
398 estimations (*e.g.* [Meghraoui and Pondrelli, 2012](#) and references therein).

399

## 400 **6. Conclusions**

401 The spatially dense crustal velocity field reported here allowed us to provide new insights into  
402 the crustal tectonic processes currently occurring in the western Mediterranean Sea. At least two  
403 main tectonic processes can be identified ([Fig. 7](#)):

404

- 405 1) We detected a slow large-scale clockwise rotation ( $\sim 0.07$  deg/Myr) of the Iberian Peninsula  
406 w.r.t. a pole located closely to the northwestern sector of the Pyrenean mountain range.  
407 Although this crustal deformation pattern could suggest a rigid rotating lithosphere block,

408 this model would predict significant shortening along the Western (off-shore Lisbon) and  
409 North Iberian margin which cannot totally ruled out but currently is not clearly observed.  
410 Conversely, we favour an interpretation that this pattern partially reflects the quasi-  
411 continuous straining of the ductile lithosphere of south-western and the western Iberia in  
412 response to viscous coupling of the mainly right lateral shear Nubia-Iberia plate boundary  
413 along the Gulf of Cádiz segment ( $n \sim 1-3.5$  for the lithosphere rheology and  $L \sim 350-500$   
414 km, Gulf of Cádiz segment), possibly superimposed on an even slower rotation-rate of  
415 Iberia.

416

417 2) The western Mediterranean basin appears fragmented into independent crustal tectonic  
418 blocks, which trapped within the Nubia-Eurasia collision, are currently accommodating  
419 most of the plate convergence rate. Based on geophysical and geological observations, these  
420 blocks are characterized by continental-type (Valencia Trough and Balears Promontory;  
421 [Pascal et al., 1992](#)), transitional-type (Alboran block; [Comas et al., 1999](#); [Torné et al., 2000](#))  
422 and oceanic-type crust (oceanic western Algerian Block; [Medaouri et al., 2014](#)). The blocks  
423 are delimited by inherited lithospheric shear structures (*e.g.*, [Acosta et al., 2002](#)). Among  
424 these blocks, the (oceanic western) Algerian one is currently acting as an indenter,  
425 transferring a fraction of the convergent rate into Eastern Betics and likely causing the  
426 eastward motion of the Balearic Promontory.

427

428 Most of the observed crustal ground deformation can be attributed to processes driven by  
429 spatially variable lithospheric plate forces imposed along the Nubia-Eurasia convergence boundary.  
430 Nevertheless, the observed deformation field infers a very low convergence rates as observed also  
431 at the eastern side of the western Mediterranean, along the Calabro Peloritan Arc, by space geodesy  
432 ([Palano, 2015](#)).

433

#### 434 **Acknowledgements**

435 PJG would like to thank Tim Wright, Richard Walters, Greg Houseman and Liam Finnerty for long  
436 and stimulating discussions. Critical comments by John Platt and Mustapha Meghraoui greatly  
437 improved the quality of this manuscript. We thank all individuals and institutions for maintain the  
438 network and providing free access to GNSS data: ARAGEA (<http://gnss.aragon.es>), BIGF  
439 ([www.bigf.ac.uk](http://www.bigf.ac.uk)), Biscay ([www.bizkaia.net](http://www.bizkaia.net)), CANTABRIA ([www.gnss.unican.es](http://www.gnss.unican.es)), CATNET  
440 ([catnet-ip.icc.cat](http://catnet-ip.icc.cat)), ERVA ([www.iev.gva.es](http://www.iev.gva.es)), EUREF ([www.epncb.oma.be](http://www.epncb.oma.be)), EUSKADI  
441 ([www.gps2.euskadi.net](http://www.gps2.euskadi.net)), GALNET ([www.cartogalicia.com](http://www.cartogalicia.com)), Gipuzkoa (<http://b5m.gipuzkoa.net>),

442 HUESCA (<http://epsh.unizar.es>), ICM  
443 (<http://www.madrid.org/cartografia/planea/cartografia/html/web/VisorGps.htm>), IDE  
444 (<http://www.iderioja.larioja.org>), IGN ([www.ign.es](http://www.ign.es)), Itacyl (<http://gnss.itacyl.es/>), RAP  
445 ([www.ideandalucia.es](http://www.ideandalucia.es)), REGAM (<http://cartomur.imida.es/regam>), Region de Murcia  
446 (<http://gps.medioambiente.carm.es>), ReNEP ([www.igeo.pt](http://www.igeo.pt)), REP ([www.rep-gnss.es](http://www.rep-gnss.es)), RGAN  
447 ([www.navarra.es](http://www.navarra.es)), RGP (<http://rgp.ign.fr>), SOPAC (<http://sopac.ucsd.edu/>), UNAVCO  
448 ([www.unavco.org](http://www.unavco.org)), XGAIB (<http://xarxagnss.caib.es>). XGAIB network is managed by SITIBSA  
449 (Servei d'Informació Territorial de les Illes Balears) Conselleria d'Agricultura, Medi Ambient i  
450 Territori (Govern de les Illes Balears). This work has been supported by the Spanish MINECO  
451 research projects AYA2010-17448 and ESP2013-47780-C2-1-R. It is a contribution for the  
452 Moncloa Campus of International Excellence.

453  
454

## 455 **Figure Captions**

456

457 **Figure 1.** Simplified tectonic map of western Mediterranean showing the main geological and  
458 structural features of Eurasia and Nubia plates. Mapped faults are redrawn from [Acosta et al., \(2002\)](#);  
459 [Asensio et al. \(2012\)](#); [García-Mayordomo et al. \(2012\)](#), [Meghraoui and Pondrelli, \(2012\)](#);  
460 [Palano et al. \(2013\)](#). Abbreviations are as follows, reporting location of major basins: Liguro-  
461 Provençal (LPB), Algero-Balearic (ABB), Alboran (AB), Valencia Trough (ValT); Massifs:  
462 Hercynian (HerM) and Moroccan Meseta (MM); Mountain Belts: Cantabrian Mountains (CanMt),  
463 Costero-Catalan Chain (CCC), Iberian Chain (IbC), Pyrenees, Atlas, Tell, Rif and Betics; Oceanic-  
464 Continent domains: Galician Bank (GaB), Gorringe Bank (GoB), Horseshoe Bank (HoB) and Gulf  
465 of Cádiz (GC); Fragmented blocks: Balears Promontory (BaIP) along Emile Baudot Escarpment  
466 (EBE), and Sardinian Corsica block (SC), and major plate boundary structures: Gloria Fault and  
467 Algerian margin. Colours and patterns represent different rock ages: 1. Neoproterozoic, 2.  
468 Paleozoic, 3. Mesozoic, 4. Tertiary-Quaternary basins, and OC, Oceanic crust.

469

470 **Figure 2.** a) Historical earthquakes (with estimated magnitude  $M \geq 5$ ;  
471 [www.emidius.eu/SHEEC/sheec\\_1000\\_1899.html](http://www.emidius.eu/SHEEC/sheec_1000_1899.html); Stucchi et al., 2013) occurred in the last  
472 millennium are reported as blue and yellow squares, for 1000 - 1899 and 1900 - 1999 time intervals,  
473 respectively. Instrumental seismicity (from 2000 up to date; [www.ign.es](http://www.ign.es)), sized as a function of  
474 magnitude and classified with different colors as a function of the focus depth, is reported as points.  
475 b) lower hemisphere, equal area projection for fault plane solutions with magnitudes of between 3.0

476 and 8.0; FPSs are colored according to rake: red indicates thrust faulting, blue is normal faulting,  
477 and yellow is strike-slip faulting.

478

479 **Figure 3.** GNSS velocities and 95 per cent confidence ellipses in a fixed Eurasian reference frame  
480 (see Supplementary Material for details).

481

482 **Figure 4.** Gray arrows represent smoothed velocities obtained by applying a median filter to all  
483 stations within 1x1 degree grid. Blue and red dashed lines represent small circles around the  
484 location of the estimated pole of rotations corresponding to the virtual Iberia w.r.t. Eurasia (blue)  
485 and Nubia w.r.t. Eurasia (red) poles. Predicted GNSS velocity vectors are shown for points along the  
486 approximate location of the plate boundary (blue Iberia-Eurasia virtual pole, and red Nubia-Eurasia  
487 pole). Note that the azimuth of the small circles, and hence the predicted motions are only aligned  
488 on a virtual line that crosses central Spain striking N30°E direction, and cutting the Nubia-Eurasian  
489 plate boundary around the Gulf of Cádiz. However, the magnitudes of the blue and red vectors  
490 disagree by about 60%. Orange lines show a simplified plate boundary.

491

492 **Figure 5.** a) NE-SW profile perpendicular velocity from the pole of rotation in stable undeformed  
493 Iberia interior the pole of rotation in to the plate boundary limit at SW Iberia (Gulf of Cádiz). Gray  
494 dots are original observed profile-parallel velocity. Black dots spatially filtered median  
495 observations. Red line is a model using box-car plate boundary condition with  $V_0=5$  mm/yr,  $L=350$   
496 km,  $n=2.5$ . Blue line represents the predicted perpendicular velocities from the estimated Iberian  
497 rotation pole model. b) Map showing the location of the selected profile (blue line). The end points  
498 of the selected profile were selected to match the inferred Iberian Euler pole and the inferred Nubia-  
499 Eurasia plate boundary zone. c) Misfit (mm/yr) plot as a function of half-wavelength,  $L$  and  $n$   
500 power-law index for the case of homogeneous boundary condition. d) Misfit (mm/yr) plot as a  
501 function of box-car length,  $L$  and  $n$  power-law index for the case of box-car boundary condition.

502

503 **Figure 6.** Detail of the GNSS velocities and 95 per cent confidence ellipses in a fixed Eurasian  
504 reference frame for the Algerian margin, Eastern Betics and Balears Promontory area.  
505 Abbreviations are: GC, Gulf of Cádiz; WAB, Western Alboran Basin; AH, Al-Hoceima; GB,  
506 Granada Basin; SN, Sierra Nevada; SF, Sierra de Filabres; TASZ, Trans-Alboran Shear Zone;  
507 EBSZ, Eastern Betics Shear Zone; YF, Yusuf Fault; EBE, Emile Baudot Escarpment.

508

509 **Figure 7.** Schematic model: main lithosphere domains are reported as irregular polygons with  
510 different colors. Eurasia, Nubia and Iberia are represented as large plates with continental and  
511 oceanic lithospheres domains. Eurasia and Iberia cannot be distinguished in terms of motion in the  
512 area of the Pyrenees, therefore they are shown as a single block with potentially variable strength,  
513 as shown the variable red shade. SW and Western Iberia is undergoing clockwise rotation that fades  
514 away towards North and Eastern Iberia. There are smaller domains in between the major plates,  
515 such as the Alboran one, which is currently undergoing clockwise rotation, internal deformation  
516 and contraction in the West and SW borders. Geodetic data indicates that the Balearic promontory  
517 is escaping to the NE, however its border structures still to be defined. Sardinia-Corsica block is  
518 consistent in motion with the Eurasian plate. Finally, convergence and interseismic coupling is  
519 variable along the Algerian margin, with a possible stronger oceanic lithosphere off-shore Oran  
520 (Western Algeria), which effectively transfer part of convergence into the SE Iberia (Eastern  
521 Betics).

522

523

## 524 **References**

- 525 Acosta, J., Muñoz, A., Herranz, P., Palomo, C., Ballesteros, M., Vaquero, M., Uchupi, E., 2001.  
526 Geodynamics of the Emile Baudot escarpment and the Balearic promontory, western  
527 Mediterranean. *Mar. Petrol. Geol.* 18, 349-369, doi:10.1016/S0264-8172(01)00003-4.
- 528 Andrieux, J., Fontbote, J.M., Mattauer, M., 1971. Sur un modèle explicatif de l'arc de Gibraltar.  
529 *Earth Planet. Sci. Lett.* 12, 191-198, doi:10.1016/0012-821X(71)90077-X.
- 530 Asensio, E., Khazaradze, G., Echeverria, A., King, R. W., Vilajosana, I., 2012. GPS studies of  
531 active deformation in the Pyrenees. *Geophys. J. Int.* 190, 913-921, doi:10.1111/j.1365-  
532 246X.2012.05525.x
- 533 Avouac, J.-P., Tapponnier P., 1993. Kinematic model of active deformation in central Asia,  
534 *Geophys. Res. Lett.* 20, 895-898, doi:10.1029/93GL00128.
- 535 Bourgois, J. A., Mauffret, A., Ammar, N. A., Demnati, N. A., 1992. Multichannel seismic data  
536 imaging of inversion tectonics of the Alboran Ridge (western Mediterranean Sea). *Geo-Mar.*  
537 *Lett.* 12, 117-122, doi:10.1007/BF02084921.
- 538 Buforn, E., Bezzeghoud, M., Udías, A., Pro, C., 2004. Seismic sources on the Iberia–African plate  
539 boundary and their tectonic implications. *Pure Appl. Geophys.* 161, 623-646,  
540 doi:10.1007/s00024-003-2466-1.
- 541 Campos, J., Maldonado, A., Campillo, A.C., 1992. Post-messinian evolutionary patterns of the  
542 central Alboran sea. *Geo-Mar. Lett.* 12, 173-178, doi:10.1007/BF02084929.



543 Cannavò, F., Palano, M., 2015. Defining Geodetic Reference Frame using Matlab: PlatEMotion 2.0.  
544 Pure Appl. Geophys., doi:10.1007/s00024-015-1112-z.

545 Casas-Sainz, A.M., De Vicente, G., 2009. On the tectonic origin of Iberian topography.  
546 Tectonophysics 474(1-2), 214-235, doi:10.1016/j.tecto.2009.01.030.

547 Comas, M.C., Platt, J.P., Soto, J.I., Watts, A.B., 1999. The origin and tectonic history of the  
548 Alboran Basin: insights from Leg 161 results. In: Zahn, R., Comas, M.C., Klaus, A. (Eds.).  
549 Proceedings of the Ocean Drilling Program, Scientific Results 161, 555-580.

550 De Lis Mancilla, F., Stich, D., Berrocoso, M., Martín, R., Morales, J., Fernandez-Ros, A., Páez, R.,  
551 Pérez-Peña, A., 2013. Delamination in the Betic Range: Deep structure, seismicity, and GPS  
552 motion. Geology 41 (3), 307-310, doi:10.1130/G33733.1.

553 Echeverría, A., Khazaradze, G., Asensio, E., Gárate J., Martín Dávila, J., Suriñach, E., 2013.  
554 Crustal deformation in eastern Betics from CuaTeNeo GPS network. Tectonophysics 608,  
555 600-612, doi:10.1016/j.tecto.2013.08.020.

556 England, P., Houseman, G., and Sonder, L., 1985, Length scales for continental deformation in  
557 convergent, divergent, and strike-slip environments: Analytical and approximate solutions for  
558 a thin viscous sheet model. J. Geophys. Res. 90, 3551-3557, doi:10.1029/JB090iB05p03551.

559 England, P.C., Jackson, J.A., 1989. Active deformation of the continents. Annu. Rev. Earth Planet.  
560 Sci. 17, 197-226, doi:10.1146/annurev.ea.17.050189.001213.

561 Fernandes, R.M.S., Miranda, J.M., Meijninger, B.M.L., Bos, M.S., Noomen, R., Bastos, L.,  
562 Ambrosius, B.A.C., Riva R.E.M., 2007. Surface velocity field of the Ibero-Maghrebian  
563 segment of the Eurasia-Nubia Plate boundary. Geophys. J. Int. 169 (1), 315-324, doi:  
564 10.1111/j.1365-246X.2006.03252.x.

565 Gárate, J., Martín-Dávila, J., Khazaradze, G., Echeverría, A., Asensio, E., Gil, A.J., de Lacy, M.C.,  
566 Armenteros, J.A., Ruiz, A.M., Gallastegui, J., Álvarez-Lobato, F., Ayala, C., Rodríguez-  
567 Caderot, G., Galindo-Zaldívar, J., Rimi, A. Harnafi, M., 2014. Topo-Iberia project: CGPS  
568 crustal velocity field in the Iberian Peninsula and Morocco. GPS Solutions 19(2), 287-295,  
569 doi:10.1007/s10291-014-0387-3.

570 García-Mayordomo, J., Insua-Arévalo, J.M., Martínez-Díaz, J.J., Jiménez-Díaz, A., Martín-Banda,  
571 R., Martín-Alfageme, S., Álvarez-Gómez, J.A., Rodríguez-Peces, M., Pérez-López, R.,  
572 Rodríguez-Pascua, M.A., Masana, E., Perea, H., Martín-González, F., Giner-Robles, J.,  
573 Nemser, E.S., Cabral J. and the QAFI Compilers Working Group (2012). The Quaternary  
574 Active Faults Database of Iberia (QAFI v.2.0). J. Iberian Geol. 38(1), 285-302,  
575 doi:10.5209/rev\_JIGE.2012.v38.n1.39219.

576 Gong, Z., van Hinsbergen, D. J. J., Dekkers, M. J., 2009. Diachronous pervasive remagnetization in  
577 northern Iberian basins during Cretaceous rotation and extension. *Earth Planet. Sci. Lett.*  
578 284(3-4), 292301, doi:10.1016/j.epsl.2009.04.039.

579 González, P.J., Tiampo, K.F., Palano, M., Cannavò, F., Fernández, J. 2012. The 2011 Lorca  
580 earthquake slip distribution controlled by groundwater crustal unloading. *Nat. Geosci.* 5, 821-  
581 825, doi:10.1038/ngeo1610.

582 Herring, T.A., 2003. MATLAB Tools for viewing GPS velocities and time series, *GPS Solutions*, 7  
583 (3), 194-199, doi:10.1007/s10291-003-0068-0.

584 Koulali, A., Ouazar, D., Tahayt, A., King, R.W., Vernant, P., Reilinger, R.E., McClusky, S.,  
585 Mourabit, T., Davila, J.M., Amraoui, N., 2011. New GPS constrains on active deformation  
586 along the Africa-Iberia plate boundary. *Earth Planet. Sci. Lett.* 308(1), 211-217,  
587 doi:10.1016/j.epsl.2011.05.048.

588 Martínez-Martínez, J. M., Booth-Rea, G., Miguel Azanon, J. M., Torcal F., 2006. Active transfer  
589 fault zone linking a segmented extensional system (Betics, southern Spain): Insight into  
590 heterogeneous extension driven by edge delamination. *Tectonophysics* 422, 159-173,  
591 doi:10.1016/j.tecto.2006.06.001.

592 Mattei, M., Cifelli, F., Martín Rojas, I., Crespo Blanc, A., Comas, M., Faccenna, C., Porreca, M.,  
593 2006. Neogene tectonic evolution of the Gibraltar Arc: New paleomagnetic constrains from  
594 the Betic chain. *Earth Planet. Sci. Lett.* 250, 522-540, doi:10.1016/j.epsl.2006.08.012.

595 Mauffret, A., Maldonado, A., Campillo, A.C., 1992. Tectonic framework of the Eastern Alboran  
596 and Western Algerian basins, Western Mediterranean. *Geo-Mar. Lett.* 12, 104-110,  
597 doi:10.1007/BF02084919.

598 McKenzie, D.P., 1970. Plate tectonics of the Mediterranean region. *Nature* 226, 239-243,  
599 doi:10.1038/226239a0.

600 Medaouri, M., Déverchère, J., Graindorge, D., Bracene, R., Badji, R., Ouabadi, A., Yelles-  
601 Chaouche, K., Bendiab, F., 2014. The transition from Alboran to Algerian basins (Western  
602 Mediterranean Sea): Chronostratigraphy, deep crustal structure and tectonic evolution at the  
603 rear of a narrow slab rollback system. *J. Geod.* 77, 186-205, doi:10.1016/j.jog.2014.01.003.

604 Meghraoui, M., Pondrelli, S., 2012. Active faulting and transpression tectonics along the plate  
605 boundary in North Africa. *Ann. Geophys.* 55 (5), doi:10.4401/ag-4970.

606 Moores, E.M., Fairbridge, R.W. 1998. *Encyclopedia of European and Asian Regional Geology.*  
607 *Encyclopedia of Earth Sciences Series*, London, 825 pp.

608 Morel, J.L., Meghraoui, M., 1996. Goringe-Alboran-Tell tectonic zone; a transpression system  
609 along the Africa-Eurasia plate boundary. *Geology* 24 (8), 755-758, doi:10.1130/0091-  
610 7613(1996)024<0755:GATTZA>2.3.CO;2.

611 Nocquet, J.M., Calais, E., 2003. Crustal velocity field of western Europe from permanent GPS array  
612 solutions, 1996-2001. *Geophys. J. Int.* 154, 72-88, doi:10.1046/j.1365-246X.2003.01935.x.

613 Palano M., González P.J., Fernández J., 2013. Strain and stress fields along the Gibraltar Orogenic  
614 Arc: constraints on active geodynamics. *Gondwana Res.* 23, 1071-1088,  
615 doi:10.1016/j.gr.2012.05.021.

616 Palano, M., 2015. On the present-day crustal stress, strain-rate fields and mantle anisotropy pattern  
617 of Italy. *Geophys. J. Int.* 200, 969-985, doi:10.1093/gji/ggu451.

618 Pascal, G., Torné, M., Buhl, P., Watts, A.B., Mauffret, A., 1992. Crustal and velocity structure of  
619 the València trough (western Mediterranean), Part II. Detailed interpretation of five Expanded  
620 Spread Profiles. *Tectonophysics* 203, 21-35, doi:10.1016/0040-1951(92)90213-P.

621 Platt, J. P., Behr, W. M., Johanesen, K., Williams, J. R., 2013. The Betic-Rif Arc and Its Orogenic  
622 Hinterland: A Review. *Annu. Rev. Earth Planet. Sci.* 41, 313-357, doi:10.1146/annurev-earth-  
623 050212-123951.

624 Perea, H., Masana, E., Santanach, P., 2012. An active zone characterized by slow normal faults, the  
625 northwestern margin of the València trough (NE Iberia): a review. *J. Iberian Geol.* 38 (1)  
626 2012: 31-52, doi:10.5209/rev\_JIGE.2012.v38.n1.39204.

627 Roest, W.R., Srivastava, S.P., 1991. Kinematics of plate boundaries between Eurasia, Iberia and  
628 Africa in the N. Atlantic from the Late Cretaceous to the present. *Geology* 19, 613-616,  
629 doi:10.1130/0091-7613(1991)019<0613:KOTPB>2.3.CO;2.

630 Rosenbaum, G., Lister, G.S., Duboz, C., 2002. Relative motions of Africa, Iberia and Europe during  
631 Alpine orogeny. *Tectonophysics*, 359, 117-129, doi:10.1016/S0040-1951(02)00442-0.

632 Sánchez-Alzola, A., Sánchez, C., Giménez, J., Alfaro, P., Gelabert, B., Gil, A.J., 2014. Crustal  
633 velocity and strain rate fields in the Balearic Islands based on continuous GPS time series  
634 from the XGAIB network (2010-2013). *J. Geod.* 82, 79-8-86, doi:10.1016/j.jog.2014.05.005.

635 Sanz de Galdeano, C., 1990. Geologic evolution of the Betic Cordilleras in the Western  
636 Mediterranean, Miocene to the present. *Tectonophysics* 172, 107-119, doi:10.1016/0040-  
637 1951(90)90062-D.

638 Sanz de Galdeano, C., García-Tortosa, F.J., Pelàez J.A., Alfaro P., Azanòn, J.M., Galindo-Zaldivar,  
639 J., Lòpez Casado, C., Lòpez Garrido, A.C., Rodríguez-Fernàndez J., Ruano P., 2012. Main  
640 active faults in the Granada and Guadix-Baza Basins (Betic Cordillera). *J. Iberian Geol.* 38,  
641 209-223, doi:10.5209/rev\_JIGE.2012.v38.n1.39215.

642 Serpelloni, E., Vannucci, G., Pondrelli, S., Argnani, A., Casula, C., Anzidei, M., Baldi, P.,  
643 Gasperini, P., 2007. Kinematics of the Western Africa-Eurasia plate boundary from focal  
644 mechanisms and GPS data. *Geophys. J. Int.* 169, 1180-1200, doi:10.1111/j.1365-  
645 246X.2007.03367.x.

646 Stich, D., Martín, J.B., Morales, J., 2007. Deformación sísmica y asísmica en la zona Béticas-Rif-  
647 Alborán. *Revista de la Sociedad Geológica de España* 20 (3-4), 311-319.

648 Stucchi et al., 2013. The SHARE European Earthquake Catalogue (SHEEC) 1000–1899. *J. Seism.*  
649 17(2), 523-544, doi:10.1007/s10950-012-9335-2.

650 Thatcher, W., 2009. How the continents deform: the evidence from tectonic geodesy. *Annu. Rev.*  
651 *Earth Planet. Sci.* 37, 237-62, doi:10.1146/annurev.earth.031208.100035.

652 Torné, M., Fernández, M., Comas, M.C., Soto, J.I., 2000. Lithospheric structure beneath the  
653 Alboran Basin: results from 3D gravity modeling and tectonic relevance. *J. Geophys. Res.*  
654 105 (B2), 3209-3228, doi: 0.1029/1999JB900281.

655 Vergés, J., Fernández, M., 2012. Tethys-Atlantic interaction along the Iberia–Africa plate boundary:  
656 The Betic-Rif orogenic system. *Tectonophysics*, 579, 144-172,  
657 doi:10.1016/j.tecto.2012.08.032.

658 Vissers, R. L. M., Meijer, P. T., 2012. Mesozoic rotation of Iberia: Subduction in the Pyrenees?.  
659 *Earth Sci. Rev.* 110(1-4), 93-110, doi:10.1016/j.earscirev.2011.11.001.

660 Whitehouse, P.L., England P.C., Houseman, G.A., 2005. A physical model for the motion of the  
661 Sierra Block relative to North America. *Earth Planet. Sci. Lett.* 237, 590-600,  
662 doi:[10.1016/j.epsl.2005.03.028](https://doi.org/10.1016/j.epsl.2005.03.028)

663 Zitellini, H.N., Gràcia, E., Matias, L., Terrinha, P., Abreu, M.A., DeAlteriis, G., Henriët, J.P.,  
664 Dañobeitia, J.J., Masson, D.G., Mulder, T., Ramella, R., Somoza, L., Diez, S., 2009. The  
665 quest for the Africa–Eurasia plate boundary west of the Strait of Gibraltar. *Earth Planet. Sci.*  
666 *Lett.* 280, 13-50, doi:[10.1016/j.epsl.2008.12.005](https://doi.org/10.1016/j.epsl.2008.12.005).

667

## **Research highlights**

An updated GNSS velocity field for Western Mediterranean.

Large-scale clockwise rotation of SW and W Iberian Peninsula w.r.t. Eurasia.

Fragmentation of the Western Mediterranean basin into crustal tectonic blocks.

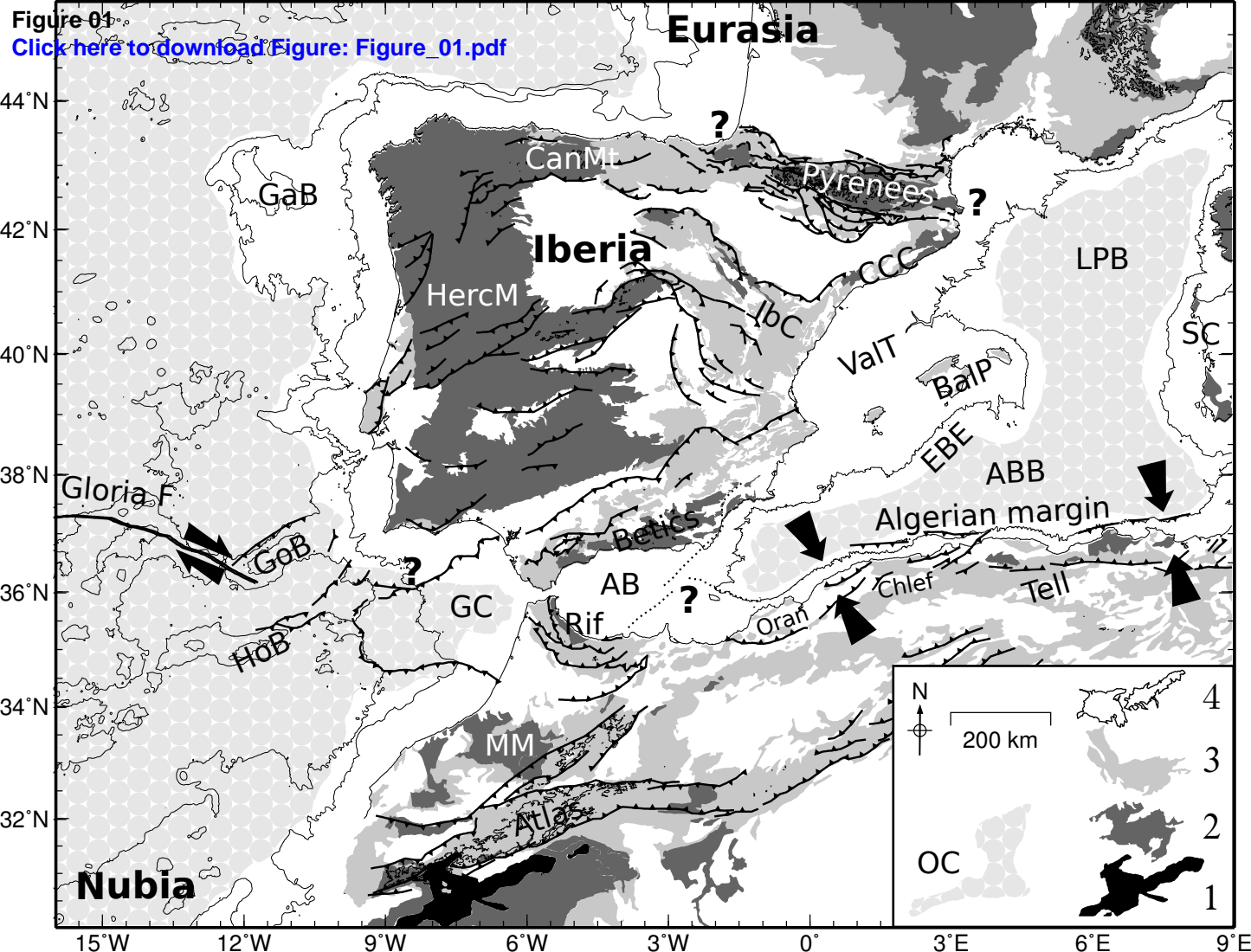


Figure 02  
[Click here to download Figure: Figure\\_02.pdf](#)

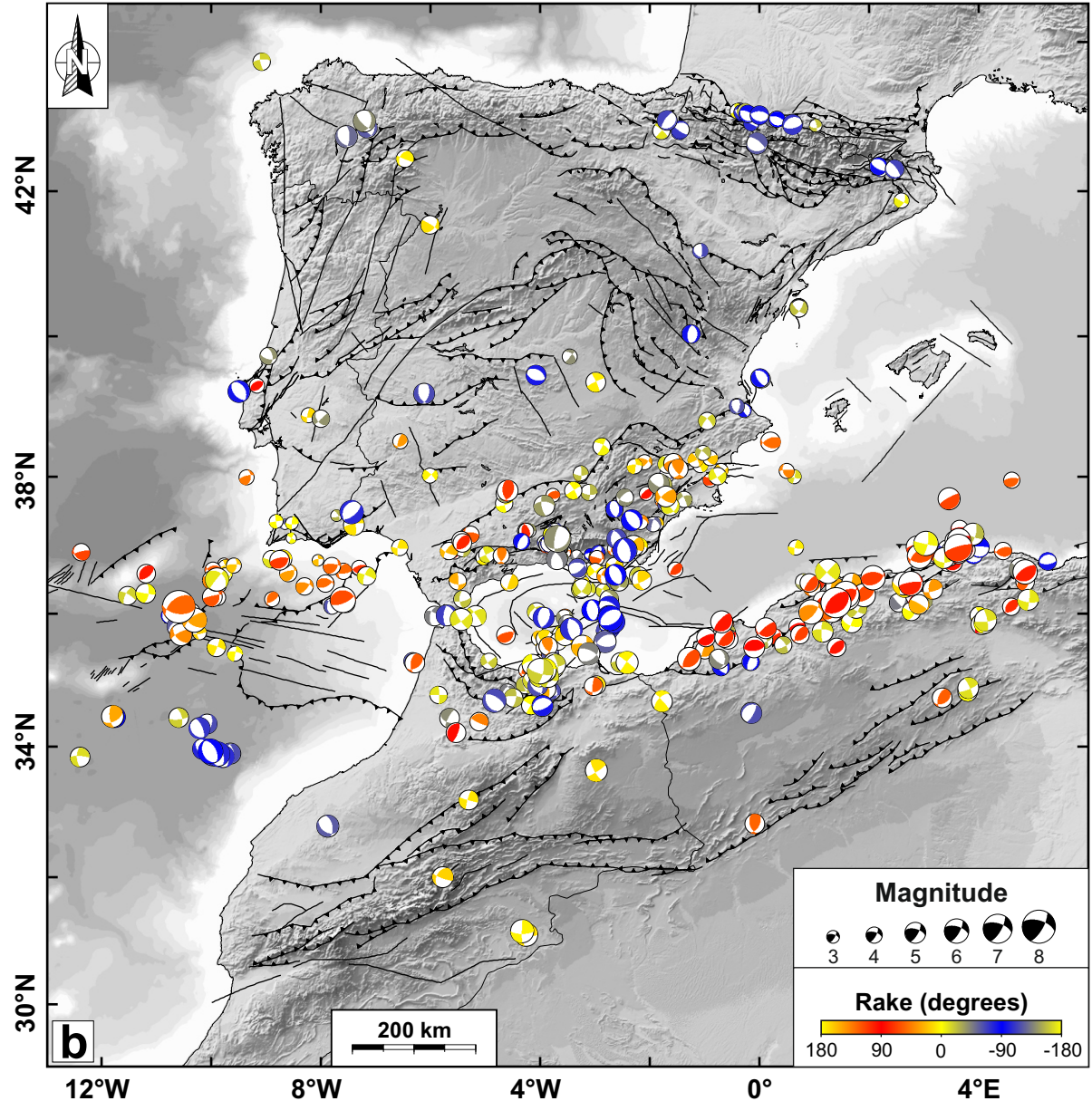
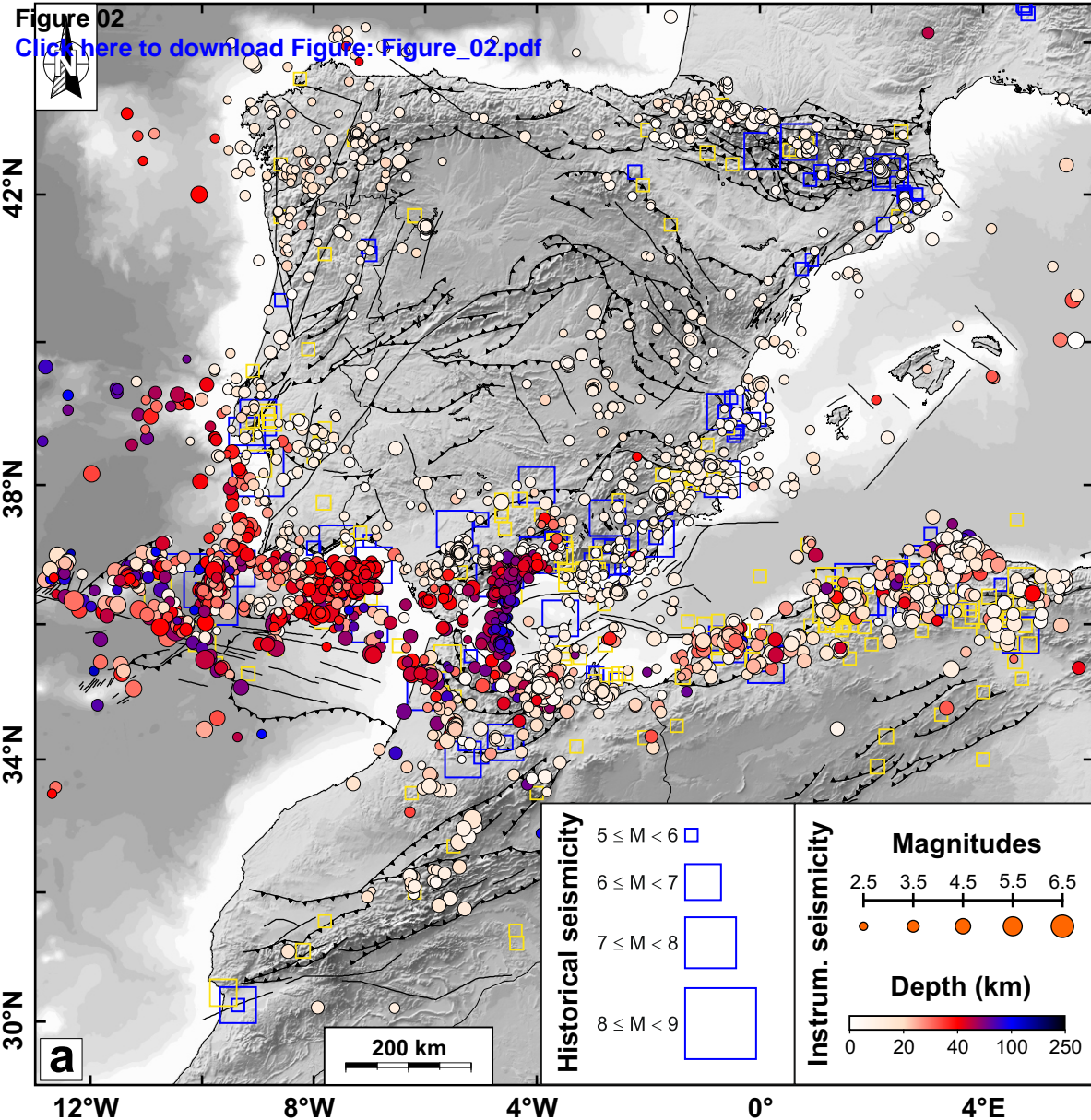
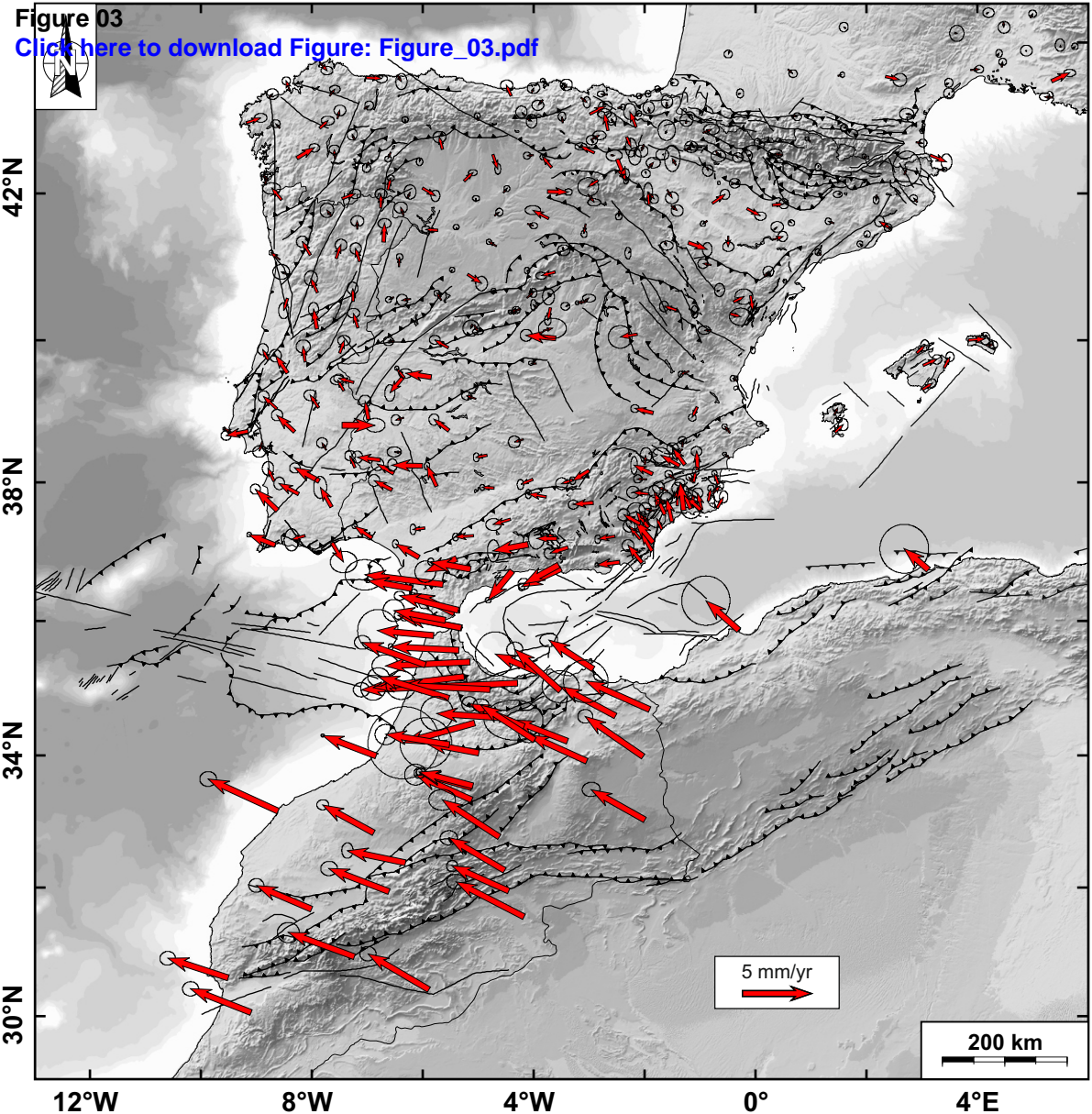


Figure 03

[Click here to download Figure: Figure\\_03.pdf](#)





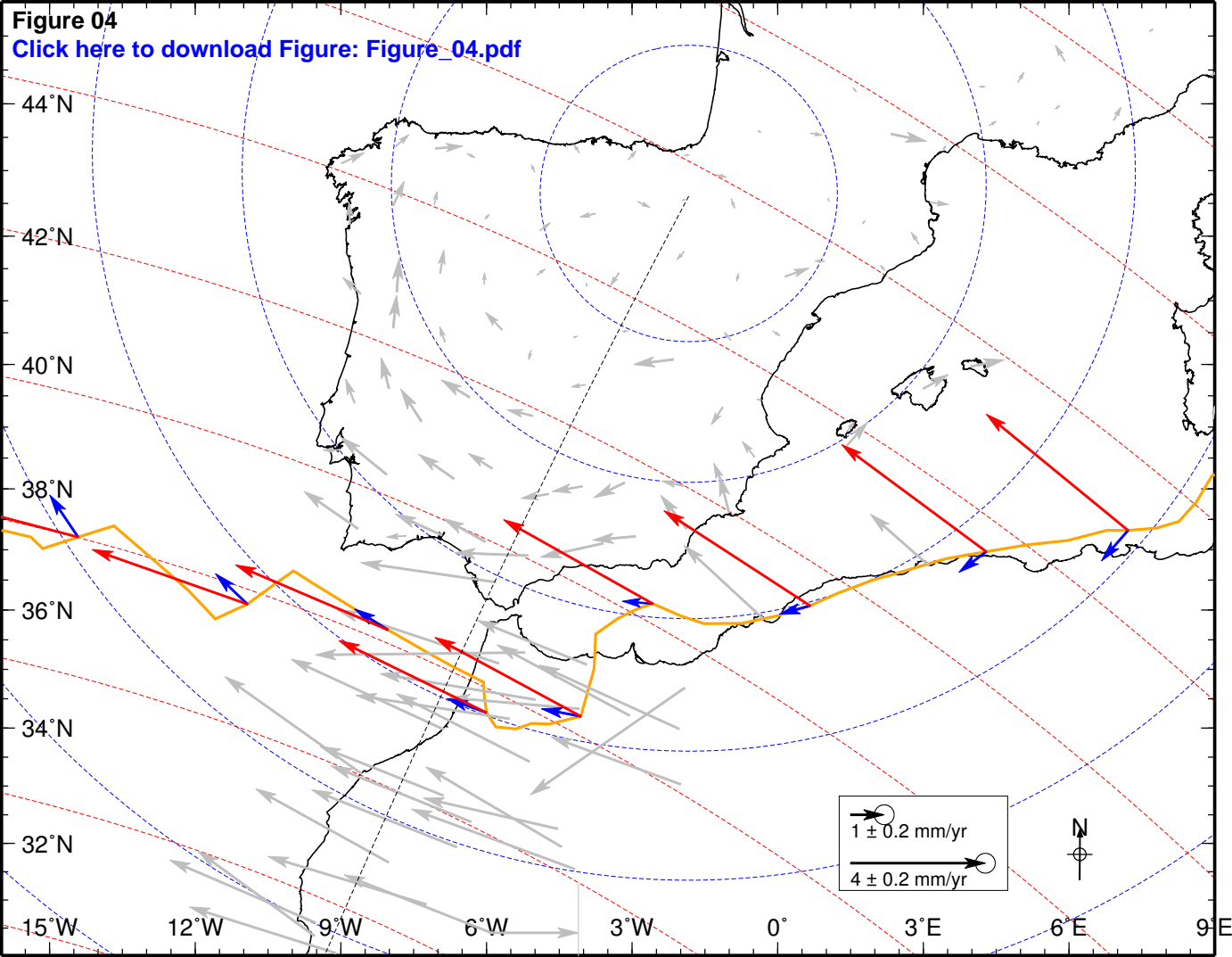


Figure 05

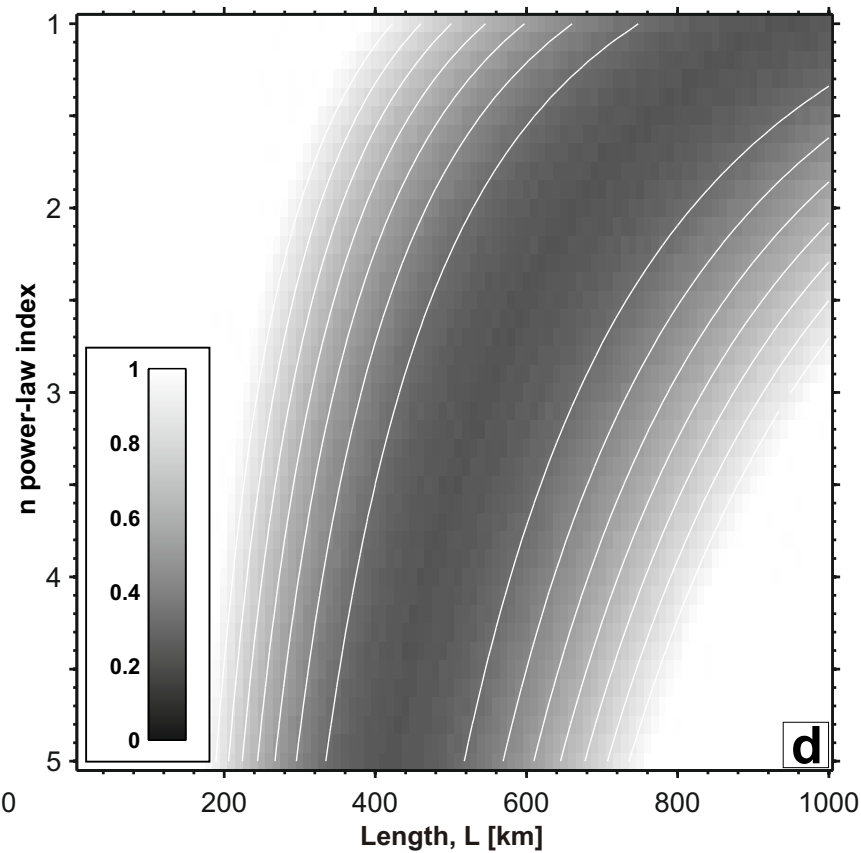
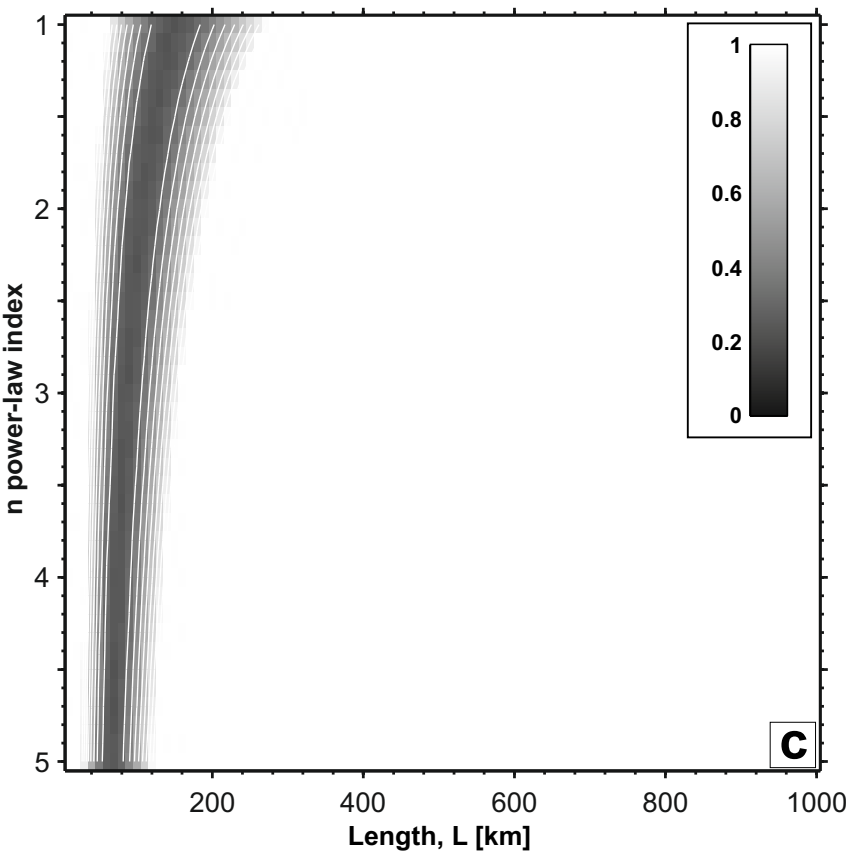
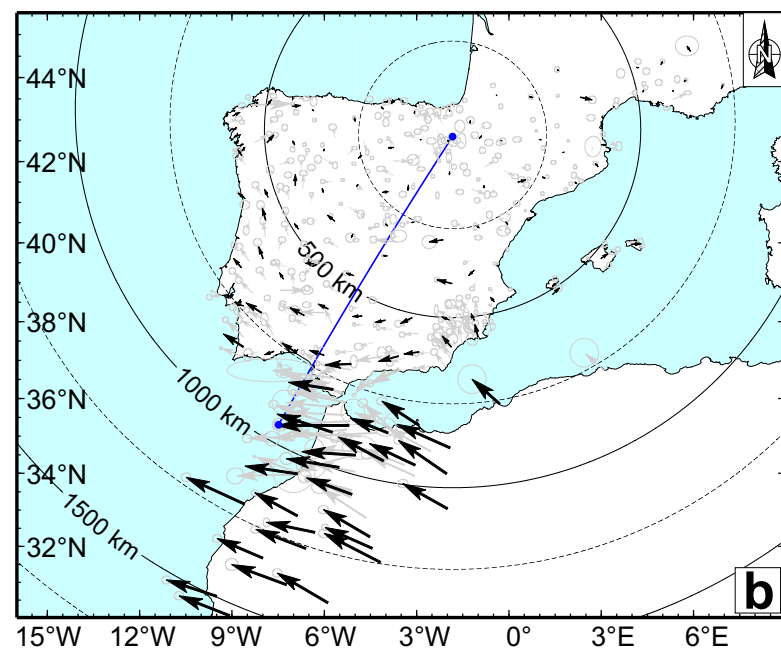
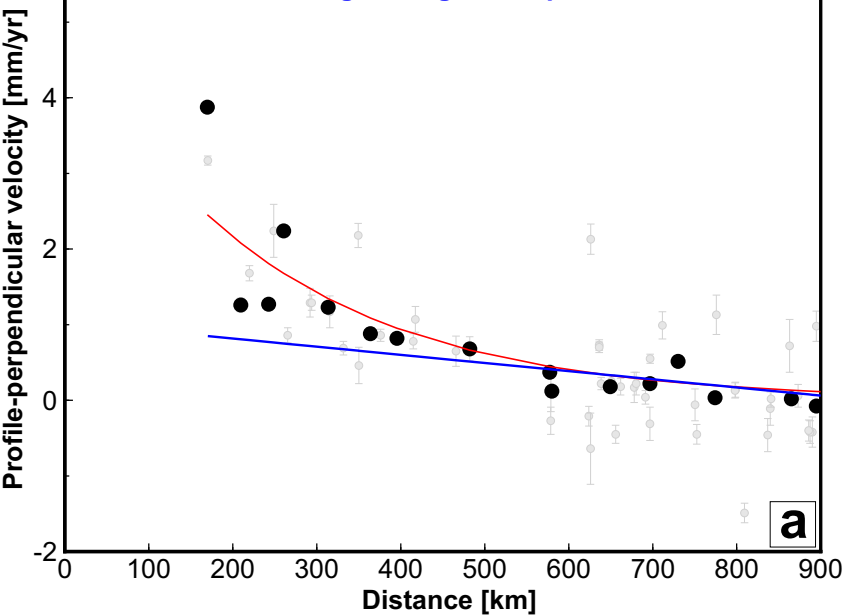
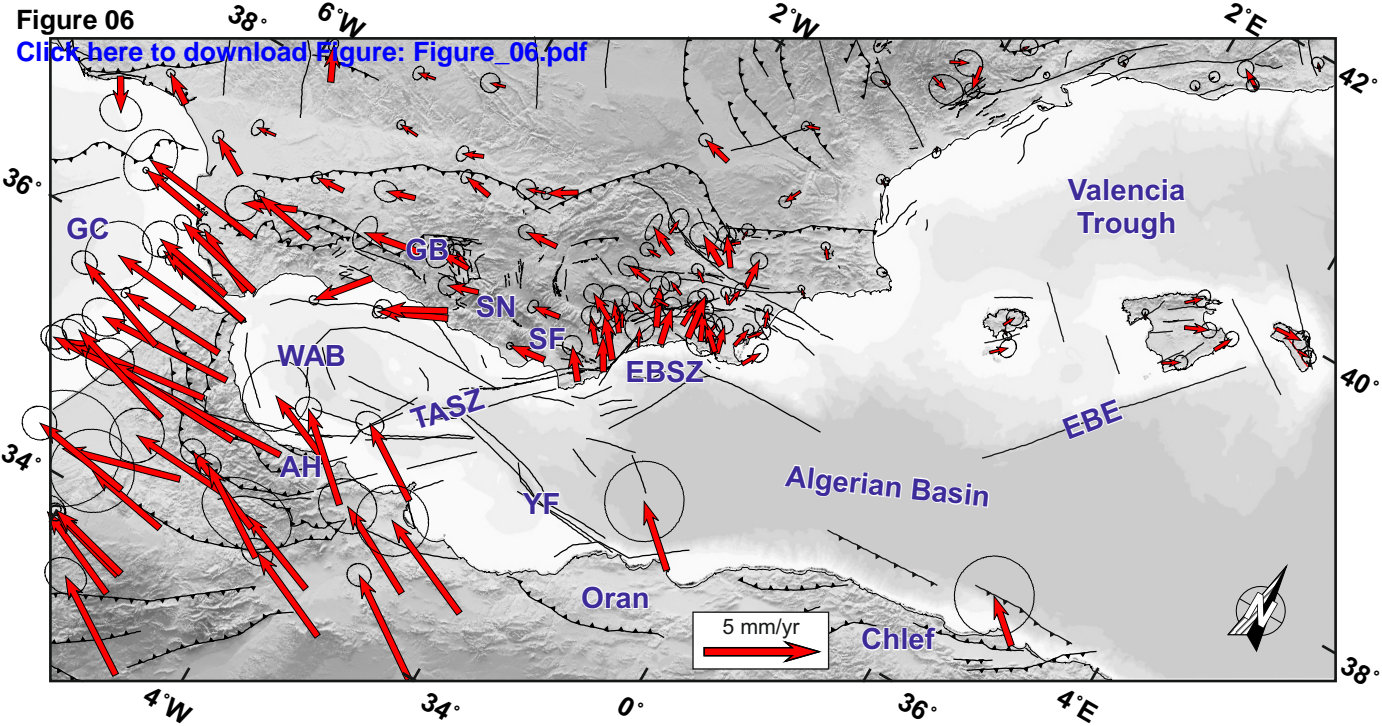
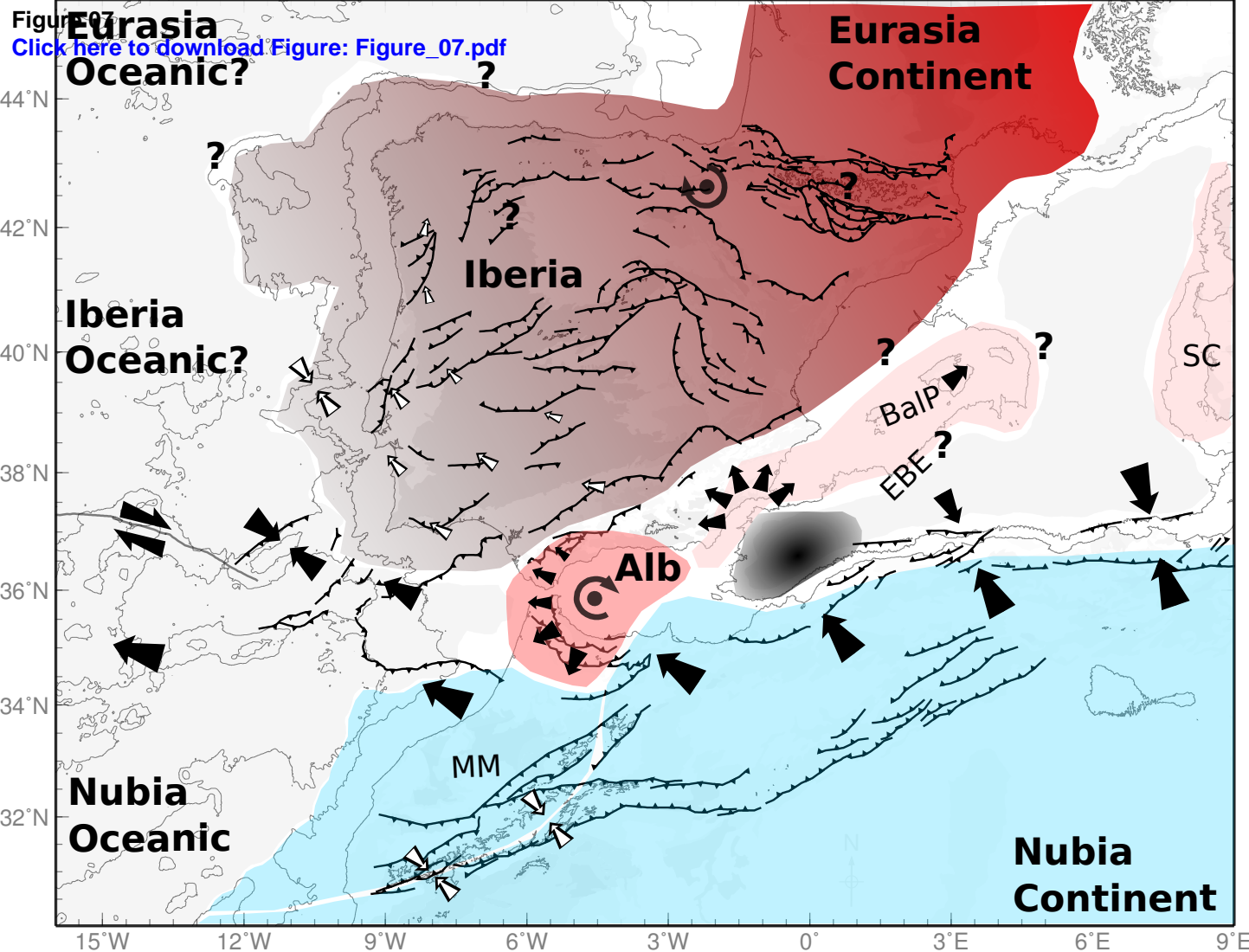
[Click here to download Figure: Figure\\_05.pdf](#)

Figure 06

[Click here to download Figure: Figure\\_06.pdf](#)





**Supplementary material for online publication only**

**[Click here to download Supplementary material for online publication only: Supplementary.Material\\_R2\\_v6.2.doc](#)**